Deep level study of Mg-doped GaN using deep level transient spectroscopy and minority carrier transient spectroscopy

Tran Thien Duc,[1,2] Galia Pozina,[1] Hiroshi Amano,[3] Bo Monemar,[1] Erik Janzén,[1] and Carl Hemmingsson[1,*]
[1]*Department of Physics, Chemistry and Biology (IFM), Linköping University, S-581 83 Linköping, Sweden*
[2]*School of Engineering Physics, Hanoi University of Science and Technology, 1 Dai Co Viet Road, Hanoi, Vietnam*
[3]*Department of Electrical Engineering and Computer Science, Nagoya University, Chikusa-ku, Nagoya, 464-8603, Japan*
(Received 18 October 2015; revised manuscript received 11 March 2016; published 25 July 2016)

Deep levels in Mg-doped GaN grown by metal organic chemical vapor deposition (MOCVD), undoped GaN grown by MOCVD, and halide vapor phase epitaxy (HVPE)-grown GaN have been studied using deep level transient spectroscopy and minority charge carrier transient spectroscopy on Schottky diodes. One hole trap, labeled HT1, was detected in the Mg-doped sample. It is observed that the hole emission rate of the trap is enhanced by increasing electric field. By fitting four different theoretical models for field-assisted carrier emission processes, the three-dimensional Coulombic Poole-Frenkel (PF) effect, three-dimensional square well PF effect, phonon-assisted tunneling, and one-dimensional Coulombic PF effect including phonon-assisted tunneling, it is found that the one-dimensional Coulombic PF model, including phonon-assisted tunneling, is consistent with the experimental data. Since the trap exhibits the PF effect, we suggest it is acceptorlike. From the theoretical model, the zero field ionization energy of the trap and an estimate of the hole capture cross section have been determined. Depending on whether the charge state is -1 or -2 after hole emission, the zero field activation energy E_{i0} is 0.57 eV or 0.60 eV, respectively, and the hole capture cross section σ_p is 1.3×10^{-15} cm^2 or 1.6×10^{-16} cm^2, respectively. Since the level was not observed in undoped GaN, it is suggested that the trap is associated with an Mg related defect.

DOI: 10.1103/PhysRevB.94.045206

I. INTRODUCTION

Due to the possibility of varying the bandgap of III–V nitrides within a broad range, GaN, and its alloys with Al and In, are today the materials of choice for fabrication of optoelectronic devices, particularly light-emitting diodes (LEDs) and ultraviolet (UV) lasers [1]. However, this would not be possible without several important development steps. Since 1969, when Maruska and Tietjen successfully synthesized GaN layers on sapphire by halide vapor phase epitaxy (HVPE) [2], there has been a great improvement of the epitaxial growth techniques. Most important is the development of effective p-type doping of GaN [3–5], which was for a long time a bottleneck in the utilization of GaN for optoelectronics and high-frequency power applications [6,7]. Magnesium (Mg) is considered so far as the only suitable dopant for fabrication of p-type GaN. Unfortunately, Mg is a relatively deep acceptor and the activation energies in the range between 0.12 and 0.25 eV have been reported depending on the doping concentration [8]. However, compared to other p-type dopants such as Zn ($E_V + 0.34$ eV) and Cd ($E_V + 0.55$ eV) [9], Mg has the lowest activation energy. Due to the large activation energy, it is necessary to introduce large Mg concentrations ($>10^{19}$ cm^{-3}) in order to get a significant free hole density at room temperature. The high Mg concentration gives rise to defect formation such as stacking faults or clusters [10–12], which is a crucial issue, especially, in case of highly p-type doped GaN [13].

Defects can give rise to deep levels in the band gap, which behave as electron traps or hole traps. These traps can affect the performance of GaN-based devices [14,15] such as reducing the quantum efficiency or shortening the lifetime. Therefore, understanding of deep levels in Mg-doped GaN is important and is a necessary requirement in order to control defects and to improve the performance of GaN-based devices. In previous studies, Auret *et al.* detected by minority charge carrier transient spectroscopy (MCTS) two hole traps with activation energies of 0.25 eV and 0.85 eV [16], respectively, in n-type GaN grown by epitaxial lateral overgrowth technique. More recently, Tokuda [17] performed MCTS studies on n-type GaN grown by metal organic chemical vapor deposition (MOCVD), and they reported three hole traps H1 ($E_V + 0.86$ eV), H2 ($E_V + 0.25$ eV), and H3 ($E_V + 0.25$ eV) in the temperature range of 100–350 K. In HVPE material, three hole traps with activation energies of 0.55 eV, 0.6 to 0.65 eV, and ~0.85 eV have been reported [18]. The latter trap with an activation energy of ~0.85 eV is commonly observed in GaN and is suggested to be related to V_{Ga} [19] or C [17]; however, its origin is still debated. Using thermal admittance and current deep-level transient spectroscopy (DLTS) on p-type Mg-doped GaN, Nakano and Jimbo reported two deep acceptor levels with activation energies of 0.135 and 0.160 eV above the valence band, respectively [20]. The levels have been associated with the Mg acceptor, and they observed that the 0.135 eV level disappears at annealing temperatures above 750 K.

In this paper, we report results of studies on deep levels in Mg-doped GaN by DLTS [21] and MCTS [22]. From these techniques, it is possible to determine important parameters of deep levels such as location in the bandgap, trap concentration, and capture cross section. One of the traps exhibits an electric field enhanced hole emission. In order to determine a zero-electric field activation energy and to understand the mechanism behind the field enhanced emission process, we have fitted the experimental data considering four theoretical models: (i) the three-dimensional (3D) Coulombic Poole-Frenkel (PF) model, (ii) the 3D square well PF model, (iii) the phonon-assisted tunneling model, and (iv) a one-dimensional (1D) Coulombic PF model including phonon-assisted tunneling.

*cah@ifm.liu.se

II. EXPERIMENTAL

Three different types of samples were used in this paper. The samples were 0.5 μm thick Mg-doped epilayers grown by MOCVD [23] on a GaN template, 3 μm undoped GaN epilayer grown by MOCVD directly on sapphire, and a GaN substrate grown by HVPE. The GaN template used for growth of the Mg-doped epilayer consists of a 200 μm thick unintentionally n-type doped GaN layer grown by HVPE on sapphire. The Mg concentration in the Mg-doped epilayer was 1.5×10^{19} cm^{-3}. The presence of hydrogen during growth electrically passivates Mg acceptors by forming Mg-H complexes. Postgrowth annealing in N_2 [24] or low-energy electron-beam irradiation (LEEBI) treatment [4] is necessary for dissociation of the Mg-H complexes and, thus, for activation of the Mg acceptors. However, in this paper, the Mg acceptors were not activated; therefore, the layer is still unintentionally n-type from the background doping.

The contacts were fabricated by thermal evaporation in which two layers of Ni/Au were used as Schottky contact with a diameter of 0.8 mm, whereas silver paint was used as Ohmic contact on the front side of the sample. The thickness of the Schottky contact is 10 nm (Ni/Au: 5/5 nm), which is sufficiently transparent to the laser with a wavelength of 355 nm. The Schottky contacts have been characterized by current-voltage (IV) measurements at room temperature using a Keithley 237 high voltage source to make sure that the leakage current is low enough (i.e., less than 10 μA) for performing reliable DLTS and MCTS measurements. The net doping concentration has been obtained from capacitance-voltage (CV) profiling using a HP 4284A LCR meter at a frequency of 1 MHz.

The DLTS and MCTS measurements allow us to study capturing and emission process of majority and minority carrier traps. In DLTS measurements, the diode is reverse biased at V_r, and short trap filling pulses with amplitude V_p are applied repeatedly as the sample temperature T is scanned. For the MCTS measurements, the trap filling pulse is replaced by an optical light pulse with an energy larger than the bandgap. Thus, both majority and minority carriers are injected in the space charge region. The carriers may be trapped in the space charge region and the electron (or hole) emission from energy levels in the depletion region is monitored as a capacitance transient following each filling pulse. The capacitance transients $C(T, t)$ are recorded at different temperatures and stored in a computer.

The DLTS and MCTS spectra are extracted from the capacitance transients according to Lang [21]. By taking the difference of the capacitance at two different time points t_1 and t_2, the spectra $S(T, t_1, t_2) = C(T,t_1) - C(T,t_2)$ are obtained. The two time points t_1 and t_2 define what we refer to as a rate window. A peak in the DLTS (or MCTS) signal $S(T, t_1, t_2)$ occurs when the capacitance transient correlates with the chosen rate window and when, from the amplitude of the peak, the concentration of defects can be obtained providing all traps are filled with carriers after the trap filling pulse. From the sign of the peak, it is possible to determine the type of trap. A positive DLTS (MCTS) peak corresponds to minority carrier trap, while a negative peak corresponds to majority carrier trap. Assuming exponential capacitance transients, it can be shown that the peak will occur at a temperature T_{peak} when the electron (hole) emission rate $e_{n(p)}$ is

$$e_{n(p)} = \ln\left(\frac{t_2}{t_1}\right) \Big/ (t_2 - t_1). \tag{1}$$

By varying t_1 and t_2, i.e., the rate window, the position of the DLTS peak occurs at different temperatures T_{peak}, which will give $e_{n(p)}(T_{\text{peak}})$. If the ratio t_1/t_2 is kept constant, it can be shown that the amplitude of the DLTS peak will be constant [25].

From the principle of detailed balance, the thermal emission rates from a deep level is given by

$$e_n(T) = g\sigma_n\langle v_n\rangle N_c \exp(-E_i/kT) \tag{2}$$

for electrons and

$$e_p(T) = g\sigma_p\langle v_p\rangle N_v \exp(-E_i/kT) \tag{3}$$

for holes. Here, g is the degeneracy factor of the trap, $\sigma_n(\sigma_p)$ the capture cross section of electrons (holes), $\langle v_n\rangle$ ($\langle v_p\rangle$) the average thermal velocity of electrons (holes), $N_c(N_v)$ is the effective density of states for the conduction (valence) band, E_i is the ionization energy, and k is the Boltzmann constant. By taking into account the thermal dependence of the average thermal velocity ($\langle v_{n,p}\rangle \propto T^{0.5}$) and the effective density of states in the band ($N_{c,v} \propto T^{1.5}$), we can determine the ionization energy and a rough estimate of the capture cross section from the slope and intercept, respectively, of the plot $\ln(e_{n,p}(T_{\text{peak}}))/T^2_{\text{peak}}$ vs $1/T_{\text{peak}}$, i.e., an Arrhenius plot.

In addition, from the amplitude of the DLTS peak $S(T_{\text{peak}})$, the concentration of defects can be obtained.

The DLTS and MCTS measurements were performed by a custom made system using a 1 MHz Boonton 7200 capacitance bridge and a 100 MHz Tabor 8024 pulse generator. For DLTS measurements on Mg-doped epilayers grown on GaN template, different reverse voltages V_r of -1.0 and 0.5 V have been applied to trace deep levels in the GaN template and in the Mg-doped layer, respectively. The filling pulse width and height was 10 ms and 0.5 V, respectively.

In MCTS measurements, different bias conditions have been used in order to measure field-enhanced emission. The reverse bias V_r was varied in the range -3 to -1 V with a step of 0.5 V and the optical filling pulse width was 10 ms. The optical filling pulse width was controlled by a model 845HP digital shutter system where it is possible to vary the exposure duration in the range of 10 ms–990 s. As light source, an Ar-ion laser with a wavelength of 355 nm was used, and the light pulse was applied on the Schottky contact at the front of the sample.

III. RESULTS AND DISCUSSION

In order to determine conductivity type and net donor concentration ($N_d - N_a$) of the samples, CV measurements were performed. From the CV-profiling measurement, it is verified that the Mg-doped layer thickness is ~500 nm and is n-type with a net donor concentration of $\sim 6 \times 10^{16}$ cm^{-3} (see inset of Fig. 1), and the HVPE grown GaN template has a net donor concentration of $\sim 3 \times 10^{16}$ cm^{-3}. The net donor concentration of the undoped epilayer grown on sapphire

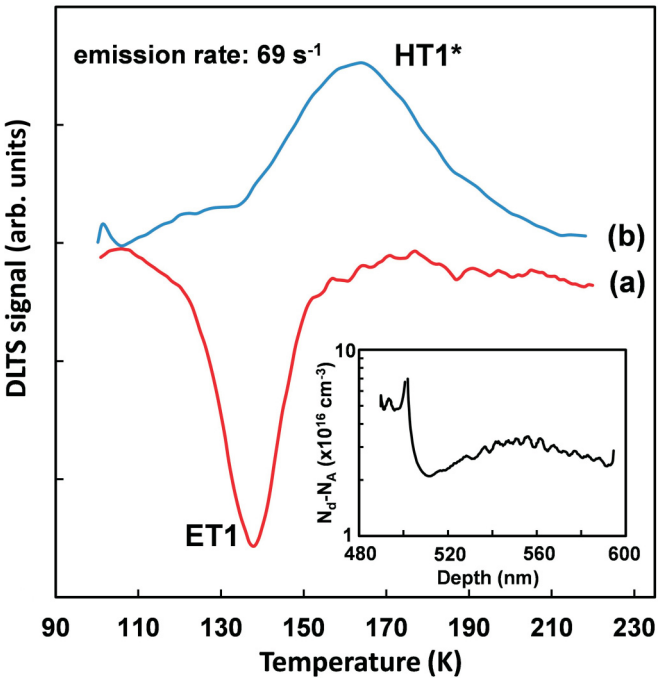

FIG. 1. The DLTS spectra of the GaN substrate (a) using a reverse bias $V_r = -1.5$ V and a filling amplitude $V_p = 0.5$ V and (b) the Mg-doped GaN layer using a reverse bias $V_r = 0.5$ V and a filling amplitude $V_p = 0.5$ V. A 69 s^{-1} boxcar rate window and a 10 ms filling pulse width was used in both cases. Inset: the net doping profile of the measured structure.

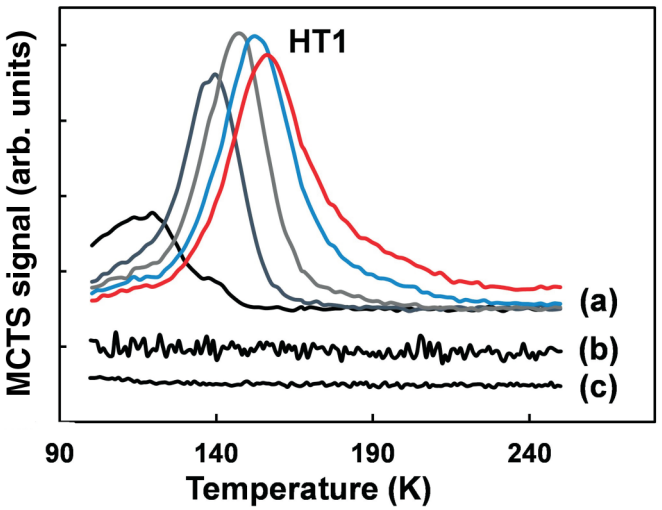

FIG. 2. The MCTS spectra of (a) Mg-doped layer using rate windows from left, 10 s^{-1},43.3 s^{-1},87 s^{-1},138.9 s^{-1}, and 172.4 s^{-1}. The optical filling pulse length (t_p) and the reverse bias (V_r) is 10 ms and −2.5 V, respectively. (b), (c) The MCTS spectra of a GaN substrate and a undoped epilayer grown on sapphire, respectively, using $V_r = -1$ V and $t_p = 100$ ms. Spectrum (a) and (b) are shifted in vertical direction for clarity.

and the HVPE grown GaN substrate was determined to 7×10^{16} cm^{-3} and 2×10^{16} cm^{-3}, respectively.

Figure 1 presents two DLTS spectra of the Mg-doped GaN sample using a filling pulse amplitude of 0.5 V and a reverse bias of −1.5 V [Fig. 1(a)] or 0.5 V [Fig. 1(b)], respectively. The used rate window is 69 s^{-1} in both cases. From the CV-profiling measurement, we determine that the depletion region width w extends to the HVPE grown GaN template for biases <-1 V. Thus, by varying the bias between −1 and −1.5 V, as shown in Fig. 1(a), we detect traps only in the GaN template. In Fig. 1(b), the bias is changing between 0.5 and 1 V, and, consequently, we detect traps only in the Mg-doped GaN layer. In Fig. 1(a), we observe one strong negative peak labeled ET1. A negative DLTS peak occurs for majority carrier emission (i.e., electron emission in n-type material). By using a reverse bias of 0.5 V and a filling pulse amplitude of 0.5 V [Fig. 1(b)], a positive broad peak, labeled HT1*, is clearly revealed. The negative peak, observed in Fig. 1(a), is absent. The observation of a positive peak, which is associated with a hole trap in n-type material, is not expected for a Schottky diode. However, minority carrier DLTS peaks using Ni Schottky n-type GaN diodes have previously been reported by Armstrong *et al.* [26]. The detection of minority carrier traps in Schottky junctions is possible for diodes with large barrier voltages since holes from the metal may be injected at the metal-semiconductor (MS) junction and get trapped [27,28]. This phenomenon has been reported even when the diode is maintained under reverse bias throughout the DLTS scan [28]. Using a conventional DLTS Arrhenius analysis described in Ref. [21], we have determined the ionization energy of the traps to 0.16 eV for both ET1 and HT1*. The electron trap ET1 detected in the HVPE grown template [Fig. 1(a)] is commonly observed in undoped n-type GaN, and it is not dependent on the growth technique [29–33]. The nature of this defect is not clear, and several suggestions are still debated. It has been proposed to be a line defect [30,34,35] or a complex of V_{Ga} with other defects [36]. Unlike ET1, the minority carrier DLTS peak HT1* has never been reported.

Thus, in order to study minority carrier traps in more details, MCTS measurements were performed on the Mg-doped layer, the HVPE grown substrate, and the undoped MOCVD grown epilayer on sapphire. Figure 2(a) shows a MCTS spectra of the Mg-doped sample using the rate windows 10 s^{-1}, 43.3 s^{-1}, 87 s^{-1}, 138.9 s^{-1}, and 172.4 s^{-1}, keeping the ratio $t_1/t_2 = 2$, an optical filling pulse width of 10 ms and a reverse bias of −2.5 V. We observe one broad peak labeled HT1. Since the peak is positive, the signal is associated with a hole trap. In MCTS measurements using illumination through the Schottky contact, it is also possible to detect electron traps within the depletion region since both holes and electrons are generated by the light pulse; however, no electron traps were observed. In order to verify that the HT1 signal is related to the Mg-doped epilayer, an MCTS measurement on the GaN substrate was performed. No hole or electron traps were observed, as can be seen in Fig. 2(b). Thus, we can conclude that the trap HT1 is related to defects solely in the Mg-doped layer. In addition, one measurement was performed on the undoped MOCVD grown epilayer on sapphire [see Fig. 2(c)]. No hole or electron traps were detected, which suggests that HT1 is related to Mg doping.

Since the ratio t_1/t_2 is constant for the different rate windows shown in Fig. 2(a), the amplitude of the MCTS peaks should be constant. However, this is not the case. The decay

of the amplitude at higher temperatures is probably related to a lower occupancy of trapped holes during the optical filling pulse. The reason for this is the upward movement of the hole quasi-Fermi level with increasing temperature, which makes the MCTS technique unsuitable for studies of deep levels at higher temperatures, see Davidson and Evans [37]. The drop of the amplitude at lower temperatures may be related on a thermal barrier for hole capturing. However, in order to determine in details the responsible process, further studies are necessary.

From a conventional one-level Arrhenius plot of the thermal emission rates, the ionization energy of trap HT1 is determined to ∼0.10 eV. However, since the HT1 peak is broad and therefore related to overlapping peaks or a continuum of hole emission processes, a conventional one-level Arrhenius analysis gives only a rough estimate of the ionization energy [35,38]. Due to the decay of the peak amplitude, the range of emission rates that can be used in the Arrhenius plot were limited.

However, it was observed that the obtained activation energies of HT1 were strongly dependent on the reverse bias V_r, and in order to study the field dependency of the hole emission rate $e_p(T,V_r)$ on V_r and temperature T in detail, MCTS measurements using different reverse biases V_r in the range −1 to −3 V were performed. From these measurements, the emission rates at $T = 150$ K, 140 K, and 120 K were extracted by changing the rate window according to Eq. (1) in order to obtain the MCTS peak at corresponding temperature. The result is illustrated in Fig. 3, which shows the hole emission rates of trap HT1 vs the electric field at the temperatures 150 K, 140 K, and 120 K. The electric field F is the field at the MS interface. Since the electric field is strongest at the MS interface, the emission rate is largest there; therefore, the MCTS signal will be dominated by hole emission from the region close to the MS interface. By varying the applied reverse bias V_r in the range −1 to −3 V, the electric field at the MS interface is varied between 6.47×10^5 V cm^{-1} and 6.87×10^5 V cm^{-1}. As can be seen in Fig. 3, by increasing the

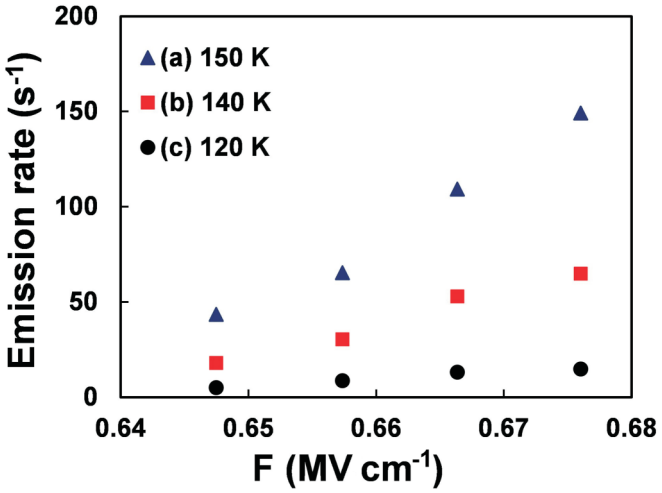

FIG. 3. Hole emission rates of trap HT1 vs electrical field F at the MS interface using different reverse biases (−1 to −3 V) at a temperature of (a) 150 K, (b) 140 K, and (c) 120 K.

electric field in the depletion region by increasing V_r, the hole emission rate increases. Thus, the hole emission rate of trap HT1 is enhanced by the electric field [39–41]. We observe a tail on the high temperature shoulder of the DLTS peaks, as seen in Fig. 2(a). Such a tail originates from nonexponential capacitance transients and can be observed when the hole emission rate is field enhanced. In this case, the hole emission rate will be highest at the MS interface, where the field is largest, and lowest at the edge of the depletion region.

Enhancement of the emission rate by an electric field is a well-known phenomenon and can be explained (as mentioned in the Introduction) by three different processes: (i) the PF effect, where the energy barrier is lowered by the presence of an electric field; (ii) the phonon-assisted tunneling process, where the probability for carrier tunneling to the conduction band (or valence band) increases by thermal energy from the lattice; and finally (iii) by pure tunneling from the trap. The PF process occurs only for charged defects while the phonon-assisted tunneling and the pure tunneling process may occur in all charge states. However, the pure tunneling process requires very large fields ($F > 10^7$ V cm^{-1}); therefore, this process is not further considered in this paper.

Considering previous studies of field enhanced emission processes [42–44], the emission rate $e(F,T)$ can generally be written as

$$e(F,T) = e_0(T)\mathrm{K}_i(F,T), \tag{4}$$

where $e_0(T)$ is the zero electric field emission rate and $\mathrm{K}_i(F,T)$ is the emission enhancement factor. The subscription i indicates the type of field enhancement model. The $e_0(T)$ is dependent only on the temperature, while $\mathrm{K}_i(F,T)$ is dependent on both temperature and electric field. By plotting the experimentally obtained emission rates $e(F,T)$ at a given temperature T vs the emission enhancement factor $\mathrm{K}_i(E,T)$, the zero field emission rate $e_0(T)$ can be extracted from the slope using simple linear regression.

Depending on the nature of the trap, the emission enhancement factor $\mathrm{K}_i(F,T)$ has to be determined. For the PF effect, Martin *et al.* [42] and Vincent *et al.* [43] proposed a Coulombic potential and a square well potential in order to describe different types of trap potentials.

Using a long range 3D Coulombic potential, the emission enhancement factor $\mathrm{K}_c(F,T)$ is described by

$$\mathrm{K}_c(F,T) = {}^1\!/_{\gamma^2}\,(e^{\gamma}(\gamma-1)+1) + \tfrac{1}{2} \tag{5}$$

where

$$\gamma = \left({}^q\!/_{k_bT}\right)\sqrt{{}^{ZqF}\!/_{\pi\epsilon_0\epsilon_r}}. \tag{6}$$

Here Z is the charge of the trap after carrier emission and ϵ_r is the dielectric constant.

In case of a short range potential, the 3D square well potential, where the depth is V_0 for $r < r_0$ and zero for $r_0 < r < \infty$, can be used in order to predict the emission rate enhancement. The 3D square well emission rate enhancement factor $\mathrm{K}_S(F,T)$ is described by

$$\mathrm{K}_S(F,T) = ({}^1\!/_{2\delta})\,(e^{\delta}-1) + \tfrac{1}{2}, \tag{7}$$

where

$$\delta = Zr_0qF/k_bT. \quad (8)$$

All parameters, except Z (the charge state of the defect after carrier emission) and the radius r_0, are known in Eq. (8). Since the two unknown parameters Z and r_0 are multiplied with each other, it is convenient to use the product $R_0 = Z^*r_0$ as a fitting parameter.

In order to describe the phonon-assisted tunneling process, Karpus and Perel [44] developed a semiclassical theory. According to the theory, the emission rate enhancement factor $K_P(F,T)$ is increasing exponentially with the square of the electric field and can be written as

$$K_P(F,T) = \exp\left(F^2/F_c^2\right), \quad (9)$$

where $F_c = \sqrt{3m^*\hbar/\tau_2^3q^2}$ is the critical electrical field.

Here m^* is the effective mass of the tunneling carrier, and τ_2 is the tunneling time, which is given by [45]

$$\tau_2 = \frac{\hbar}{2k_bT} \mp \tau_1, \quad (10)$$

where the minus or plus sign corresponds to a weak or strong electron-phonon coupling, respectively [45]. The magnitude of the time constant τ_1 is on the order of the inverse local impurity vibration frequency and is practically independent of the temperature [46]. Thus, in order to determine the emission rate enhancement factor for the phonon-assisted tunneling process, the time constant τ_1 has to be determined, and in most cases, τ_1 is used as a fitting parameter.

Vincent *et al.* suggested a 1D model taking into account both the Coulombic PF effect and phonon-assisted tunneling [43]. They showed that for a Coulomb potential, both the PF effect and phonon-assisted tunneling are important at the field range we are studying ($\sim 10^5$ V cm^{-1}). Additionally, Ganichev *et al.* [47] have shown that in the range of moderate electric fields (10^4–10^5 V cm^{-1}), the phonon-assisted tunneling process is in most cases the dominant mechanism for electric field enhancement of the emission rate. The 1D Coulombic PF model, which includes phonon-assisted tunneling $K_{CP}(F,T)$, is described by

$$K_{CP}(F,T) = \exp\left(\frac{\Delta E_i}{k_bT}\right) + \int_{\Delta E_{i/k_bT}}^{E_{i0/k_bT}} \exp \left\{ z - z^{3/2}\left(\frac{4}{3}\right)\frac{\sqrt{m^*}}{q\hbar F}(k_bT)^{3/2} \times \left(1 - \left(\frac{\Delta E_i}{zk_bT}\right)^{5/3}\right)\right\} dz, \quad (11)$$

where

$$\Delta E_i = q\sqrt{\frac{zqF}{\pi\epsilon_0\epsilon_r}} \quad (12)$$

is the change in the 1D potential barrier due to the presence of the field and E_{i0} is the zero field ionization energy of the trap. Since E_{i0} is an unknown parameter, it is used as a fitting parameter to the experimental data.

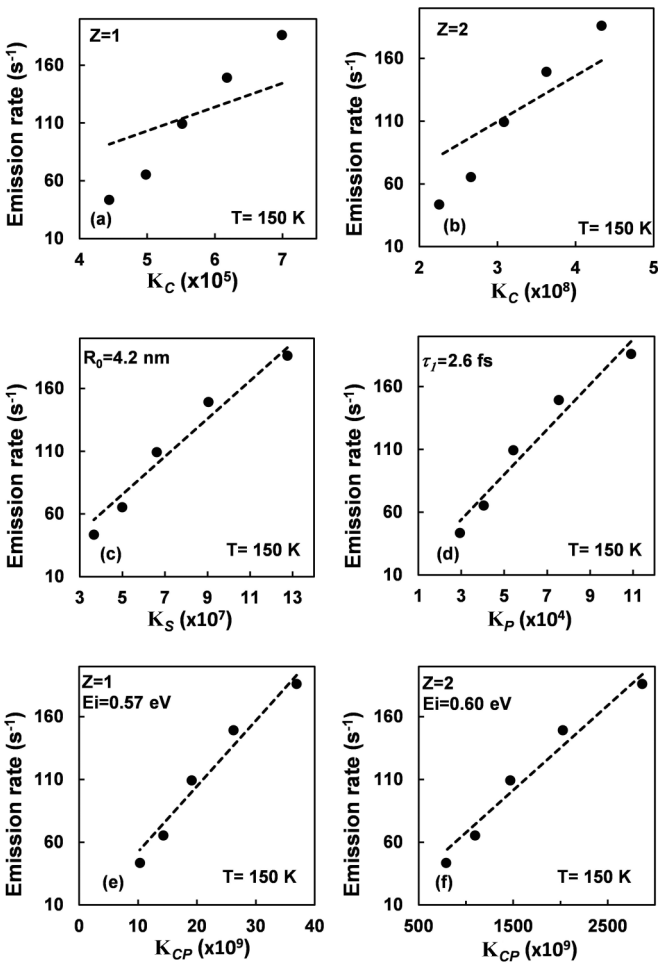

FIG. 4. Hole emission rates of trap HT1 vs field enhancement factors at a temperature of 150 K. The 3D Coulombic PF model using charge state $Z = 1$ (a) and $Z = 2$ (b). Square well PF model (c), phonon-assisted tunneling model (d), and 3D Coulombic PF model including phonon-assisted tunneling using $Z = 1$ (e) and $Z = 2$ (f). The fitted result is shown with the dotted line.

The zero field emission rates $e_0(T)$ were extracted from the dependence of the experimentally obtained emission rates $e(F,T)$ according to Eq. (4). In case of the 3D Coulombic PF model, K_C was directly calculated using Eq. (5), while for the other emission enhancement factors, the unknown parameters was fitted to the experimentally obtained emission rates. For K_S (square well PF model), K_P (phonon-assisted tunneling process), and K_{CP} (1D Coulombic PF model including phonon-assisted tunneling), the parameters R_0, time constant τ_1, and ionization energy E_{i0}, respectively, have been fitted under the assumption that they are independent on the electric field and temperature. For the 3D Coulombic PF model Eq. (4) and the 1D Coulombic PF model with phonon-assisted tunneling Eq. (11), three different charge states $Z = 1$, $Z = 2$, and $Z = 3$ were investigated.

Figure 4 shows a plot of hole emission rate vs emission enhancement factors at 150 K for six different cases. The fitted result is shown with the dotted line. Figures 4(a) and 4(b) show the 3D Coulombic PF model using the charge states $Z = 1$ and $Z = 2$, respectively. As can be seen, the fitting result is poor

TABLE I. The zero field ionization energy E_{i0} and the capture cross section σ_p.R_0, τ_1, and E_{i0} are fitting parameters used for the square well PF potential, phonon-assisted tunneling model, and the 1D Coulombic PF model including phonon-assisted tunneling, respectively. Z indicates the assumed charge state of the trap after hole emission.

Model	Z	E_{i0} (eV)	σ_p(cm^2)	R_0(nm)	τ_1(fs)
Phonon-assisted tunneling	–	0.60	3.9×10^{-9}	–	2.6
PF square well potential	1	0.35	1.4×10^{-20}	4.2	–
PF Coulombic pot. with	1	0.57	1.3×10^{-15}	–	–
phonon-assisted tunneling	2	0.60	1.6×10^{-16}	–	–
	3	0.62	8.1×10^{-16}	–	–

for both charge states, and for higher charge states ($Z > 2$), the fitting is not improved (not shown); therefore, we will not further consider this model.

For the other models, we obtain the fitting parameters R_0, τ_1, and E_{i0} for the square well PF model, phonon-assisted tunneling model and 1D Coulombic PF model including phonon-assisted tunneling, respectively. Using Eq. (3), we can directly calculate the hole capture cross sections σ_h for the 1D Coulombic PF model including phonon-assisted tunneling. The obtained values are presented in Table I.

Further analysis is necessary in order to determine the zero field ionization energies and hole capture cross sections for the phonon-assisted tunneling model and the square well PF model. The zero field thermal emission rate $e_0(T)$ is described by Eq. (3), and by plotting the logarithm of $e_0(T)$ vs $1/T$ an Arrhenius plot is obtained:

$$\ln(e_0(T)) = \ln(g\sigma_p\langle v_p\rangle N_v) - E_{i0}/kT. \quad (13)$$

By taking into account temperature dependencies of the thermal velocity ($\langle v_p\rangle \propto T^{0.5}$) and the effective density of states in the valence band ($N_v \propto T^{1.5}$), the zero field ionization energy E_{i0} and an estimate of the hole capture cross sections σ_p were obtained from the slope and intercept, respectively (see Fig. 5). The obtained values are presented in Table I.

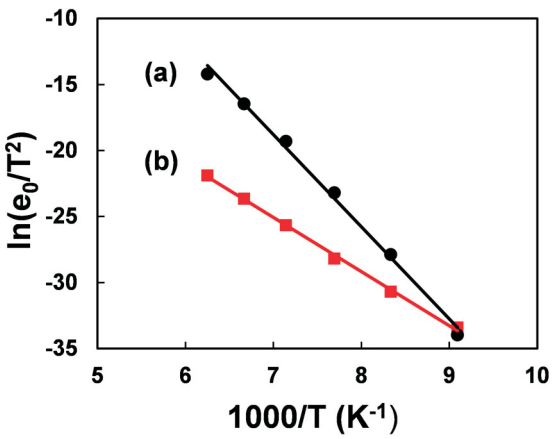

FIG. 5. Arrhenius plots of the zero electric field T-square corrected emission rate e_0/T^2 vs 1000/T using (a) the phonon-assisted tunneling model and (b) the square well PF model.

By using the phonon-assisted tunneling model, we obtain a positive sign of τ_1, which indicates, according to Ganichev *et al.* [47], a strong electron-phonon coupling. Interesting to note is the large variation of the hole capture cross section from very large ($\sim 10^{-9}$ cm^2) using the phonon-assisted tunneling model to very small ($\sim 10^{-20}$ cm^2) for the square well PF model.

Figure 6 shows the experimental and theoretical emission rates (dotted lines) obtained from the fittings for the square well PF model, phonon-assisted tunneling model, and the 1D Coulombic PF model, including phonon-assisted tunneling using the two charge states $Z = 1$ and $Z = 2$ at 120 K, 140 K, and 150 K vs the electrical field. As can be seen, the result reveals that the experimental data are in good agreement with the square well PF model [Fig. 6(b)] and the 1D Coulombic PF models, which includes phonon-assisted tunneling using the two charge states $Z = 1$ and $Z = 2$ [Figs. 6(c) and 6(d)]. For higher charge states ($Z > 2$), the fitting results are increasingly deviating from the experimental data (not shown). In the case of the pure phonon-assisted tunneling model [Fig. 6(a)], the model increasingly underestimates the emission rates with reducing temperature.

For the square well PF model [Fig. 6(b)], the fit is good; however, the model gives a very small capture cross section ($\sigma_p = 1.4 \times 10^{-20}$ cm^2), which is normally associated with traps related to a neutral (or even repulsive) centers. In that case, we would not expect any PF effect. We conclude that the fitting using PF models without phonon-assisted tunneling gives unreasonable results. Thus, we suggest that the observed field enhancement is related to both phonon-assisted tunneling and a PF mechanism, and it is necessary to include both processes in the model. A field enhanced emission rate from a hole trap level suggests that the level is acceptorlike. Thus, according to our results, level HT1 is associated with a deep acceptor level. The fitting is good for both charge states $Z = 1$ and $Z = 2$; however, for a defect with the charge state $Z = 2$, the capture cross section is expected to be large. Although the obtained capture cross section of 1.6×10^{-16} cm^2 (see Table I) seems to be a bit too small, we cannot rule out that the charge state of the trap is $Z = 2$, and additional studies are necessary in order to clarify the charge state. Thus, according to our results, HT1 is associated with a deep acceptor level at 0.57 eV ($Z = 1$) or 0.60 eV ($Z = 2$) above the valence band, with a hole capture cross section $\sigma_p \sim 1.3 \times 10^{-15}$ cm^2 or $\sim 1.6 \times 10^{-16}$ cm^2, respectively.

We now consider the minority carrier peak HT1* with an ionization energy of 0.16 eV [see Fig. 1(b)]. Since peak HT1* is associated with hole trapping at the MS interface, the hole emission process occurs where the electric field is largest. In the measurement, a reverse bias V_r of 0.5 V was used, which give rise to a maximum electric field of 6.25×10^5 V cm^{-1} at the MS interface. By calculating the expected ionization energy of HT1 using $F = 6.25 \times 10^5$ V cm^{-1}, we conclude that the ionization energy of HT1* is similar to HT1 at this field; therefore, we suggest that the peak HT1 and HT1* are both associated with the same trap.

There have been several investigations on Mg-doped GaN after activation of the Mg dopants, but the data on unactivated Mg in GaN is scanty. However, Zhu *et al.* [48] presented a DLTS study on the effect of thermal annealing on hole traps

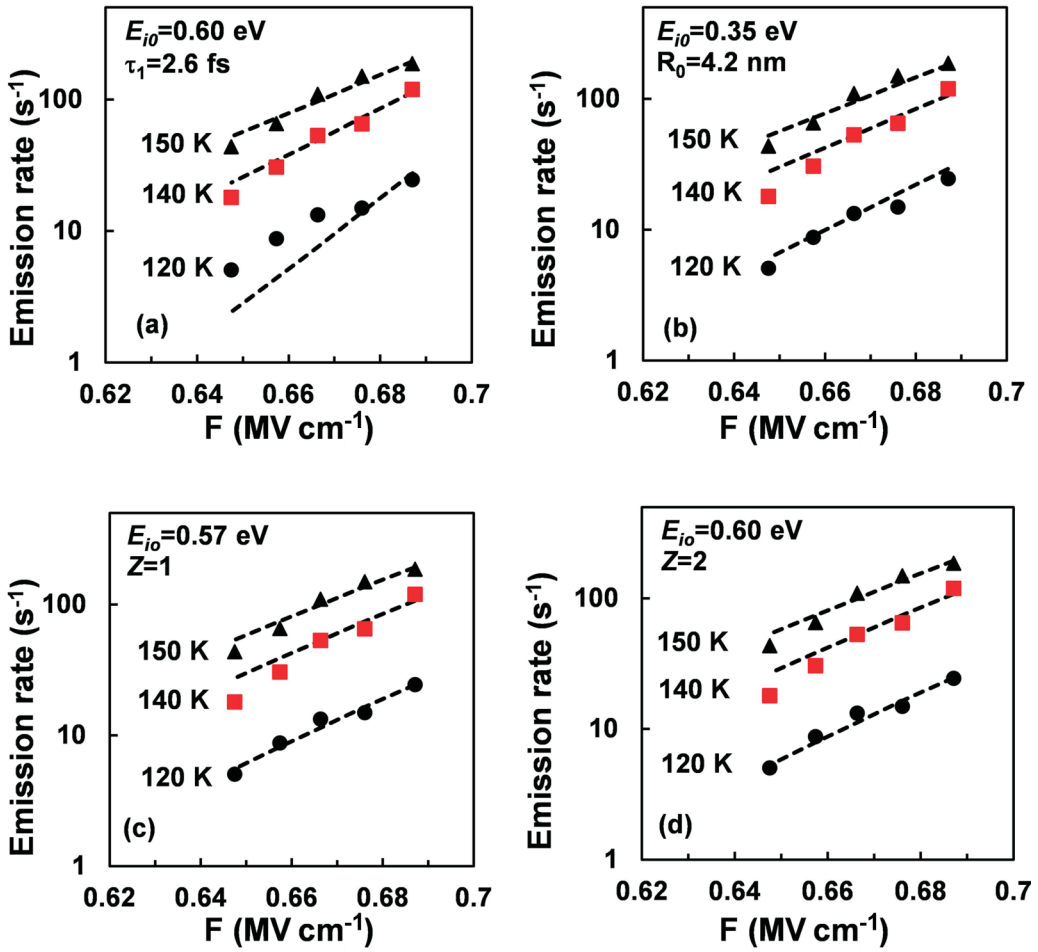

FIG. 6. Experimental and fitted emission rates (dotted lines) of HT1 vs electric field F. The theoretical values were obtained from the zero field activation energies using (a) the phonon-assisted tunneling model, (b) the 3D square well PF model, (c) the 1D Coulombic model including phonon-assisted tunneling assuming a trap charge state of (c) $Z = 1$, and (d) $Z = 2$ at the temperature of 120 K, 140 K, and 150 K, respectively.

in Mg-doped GaN grown by MOCVD. No measurements was performed on the unactivated as-grown sample; however, after a relatively short annealing of 20 min at 800 °C in N_2, they observed a broad peak in the same temperature range as HT1 with an activation energy and hole capture cross section of 0.41 eV and 5.2×10^{-13}cm^{-2}, respectively. By numerical fitting, they decomposed the broad peak into five single trap levels. After 40 min annealing at 800° C in N_2, two of the trap levels were annealed out, and after additional 10 min annealing, only one trap level remained with an activation energy of 0.20 eV and a hole capture cross section of 1.9×10^{-17}cm^{-2}. They attributed the annealing process to removal of hydrogen, and the multiple trap levels were discussed in terms of the Mg-N-H complex [49,50]. In the study of Zhu *et al.* field enhanced emission processes were not investigated. Since the hole emission rate of HT1 exhibit a strong electrical field dependence, it is difficult to compare activation energy data obtained from space charge measurement techniques such as DLTS and MCTS. However, the activation energy of the trap should be less than the zero field activation energy of 0.57–0.60 eV. Considering this, the activation energy of the Mg related broad peak observed after 20 min annealing reported by Zhu *et al.* [48] corresponds well with peak HT1. Thus, HT1 may be related to the Mg-N-H complex.

IV. CONCLUSION

In this investigation, Mg-doped GaN layers grown by MOCVD were electrically characterized using DLTS and MCTS. One hole trap HT1 (HT1*) with an electric field dependent ionization energy and an electron trap ET1 ($E_C - 0.16$ eV) were detected in the Mg-doped layer and in the substrate, respectively, in the temperature range 80–300 K.

In order to study the electric field enhanced emission process, four different models, the 3D Coulombic PF model, the 3D square well PF model, the phonon-assisted tunneling model, and a 1D Coulombic PF model, including phonon-assisted tunneling, was used. By fitting the MCTS data to the models, it was concluded that both PF effect and phonon-assisted tunneling have to be considered in order to describe the experimental data. Using the Coulombic PF model, including phonon-assisted tunneling, the zero field ionization energy E_{i0} of trap HT1 was determined to 0.57 eV

or 0.60 eV, depending on whether the charge state is −1 or −2, respectively, after hole emission. The hole capture cross section σ_p of HT1 was determined to 1.3×10^{-15} cm^2 if the charge state is −1 and 1.6×10^{-16} cm^2 if the charge state is −2 after emission. Since the PF has to be included in the model, we suggest that the trap is acceptorlike. Considering that the HT1 trap was only observed in the Mg-doped layer, we suggest that the HT1 level is associated with the Mg doping.

ACKNOWLEDGMENT

This research was supported by Swedish Research Council (Grant No. 621-2010-3850) and Swedish Energy Agency (Grant No. 38338-1).

[1] B. S. Nakamura and M. R. Krames, Proc. IEEE **101**, 2211 (2013).
[2] H. P. Maruska and J. J. Tietjen, Appl. Phys. Lett. **15**, 327 (1969).
[3] A. Dussaigne, B. Damilano, J. Brault, J. Massies, E. Feltin, and N. Grandjean, J. Appl. Phys. **103**, 013110 (2008).
[4] H. Amano, M. Kito, K. Hiramatsu, and I. Akasaki, Jpn. J. Appl. Phys. **28**, L2112 (1989).
[5] M. Rubin, N. Newman, J. S. Chan, T. C. Fu, and J. T. Ross. Appl. Phys. Lett. **64**, 64 (1994).
[6] D. W. Runton, B. Trabert, J. B. Shealy, and R. Vetury, IEEE Microw. Mag. **14**, 82 (2013).
[7] S. J. Pearton, J. C. Zolper, R. J. Shul, and F. Ren, J. Appl. Phys. **86**, 1 (1999).
[8] S. Brochen, J. Brault, S. Chenot, A. Dussaigne, M. Leroux, and B. Damilano, Appl. Phys. Lett. **103**, 269904 (2013).
[9] S. Fischer, C. Wetzel, and E. E. Haller, Appl. Phys. Lett. **67**, 1298 (1995).
[10] G. Pozina, C. Hemmingsson, P. P. Paskov, J. P. Bergman, B. Monemar, T. Kawashima, H. Amano, I. Akasaki, and A. Usui, Appl. Phys. Lett. **92**, 151904 (2008).
[11] S. Khromov, B. Monemar, V. Avrutin, X. Li, H. Morkoç, L. Hultman, and G. Pozina, Appl. Phys. Lett. **100**, 172108 (2012).
[12] S. Khromov, D. Gregorius, R. Schiller, J. Lösch, M. Wahl, M. Kopnarski, H. Amano, B. Monemar, L. Hultman, and G. Pozina, Nanotechnology **25**, 275701 (2014).
[13] S. Khromov, C. G. Hemmingsson, H. Amano, B. Monemar, L. Hultman, and G. Pozina, Phys. Rev. B **84**, 075324 (2011).
[14] O. Toshio and A. Masaharu, Jpn. J. Appl. Phys. **19**, 2395 (1980).
[15] D. O. Demchenko, I. C. Diallo, and M. A. Reshchikov, Phys. Rev. Lett. **110**, 087404 (2013).
[16] F. D. Auret, W. E. Meyer, L. Wu, M. Hayes, M. J. Legodi, B. Beaumont, and P. Gibart, Phys. Status Solidi A **201**, 2271 (2004).
[17] Y. Tokuda, Proceedings of CS ManTech Conference, 19–22 May, 2014, Denver, Colorado, USA, pp. 19–24 (unpublished).
[18] A. Y. Polyakov, I. H. Lee, N. B. Smirnov, A. V. Govorkov, E. A. Kozhukhova, and S. J. Pearton, J. Appl. Phys. **109**, 123701 (2011).
[19] A. Hierro, D. Kwon, S. A. Ringel, M. Hansen, J. S. Speck, U. K. Mishra, and S. P. DenBaars, Appl. Phys. Lett. **76**, 3064 (2000).
[20] Y. Nakano and T. Jimbo, J. Appl. Phys. **92**, 5590 (2002).
[21] D. V. Lang, J. Appl. Phys. **45**, 3023 (1974).
[22] R. Brunwin, B. Hamilton, P. Jordan, and A. R. Peaker, Electron. Lett. **15**, 349 (1979).
[23] G. Pozina, P. P. Paskov, J. P. Bergman, C. Hemmingsson, L. Hultman, B. Monemar, H. Amano, I. Akasaki, and A. Usui, Appl. Phys. Lett. **91**, 221901 (2007).
[24] S. Nakamura, T. Mukai, M. Senoh, and N. Iwasa, Jpn. J. Appl. Phys. **31**, L139 (1992).
[25] D. K. Schroder, *Semiconductor Material and Device Characterization* (John Wiley & Sons, New Jersey, 2006).
[26] A. Armstrong, A. R. Arehart, D. Green, U. K. Mishra, J. S. Speck, and S. A. Ringel, J. App. Phys. **98**, 053704 (2005).
[27] F. D. Auret and M. Nel, J. Appl. Phys. **61**, 2546 (1987).
[28] L. Stolt and K. Bohlin, Solid. State. Electron. **28**, 1215 (1985).
[29] P. Hacke, T. Detchprohm, K. Hiramatsu, N. Sawaki, K. Tadatomo, and K. Miyake, J. Appl. Phys. **76**, 304 (1994).
[30] E. Płaczek-Popko, J. Trzmiel, E. Zielony, S. Grzanka, R. Czernecki, and T. Suski, Phys. B Condens. Matter **404**, 4889 (2009).
[31] Y. Tokuda, Y. Matsuoka, H. Ueda, O. Ishiguro, N. Soejima, and T. Kachi, Superlattices Microstruct. **40**, 268 (2006).
[32] C. D. Wang, L. S. Yu, S. S. Lau, E. T Yu, and W. Kim, Appl. Phys. Lett. **72**, 1211 (1998).
[33] T. T. Duc, G. Pozina, E. Janzén, and C. Hemmingsson, J. Appl. Phys. **114**, 153702 (2013).
[34] H. K. Cho, C. S. Kim, and C.-H. Hong, J. Appl. Phys. **94**, 1485 (2003).
[35] C. B. Soh, S. J. Chua, H. F. Lim, D. Z. Chi, S. Tripathy, and W. Liu, J. Appl. Phys. **96**, 1341 (2004).
[36] Z.-Q. Fang, D. C. Look, and L. Polenta, J. Phys. Condens. Matter **14**, 13061 (2002).
[37] J. A. Davidson and J. H. Evans, J. Appl. Phys. **81**, 251 (1997).
[38] P. Omling, E. R. Weber, L. Montelius, H. Alexander, and J. Michel, Phys. Rev. B **32**, 6571 (1985).
[39] A. O. Evwaraye, S. R. Smith, W. C. Mitchel, and G. C. Farlow, J. Appl. Phys. **106**, 063702 (2009).
[40] U. S. Qurashi, M. Z. Iqbal, C. Delerue, and M. Lannoo, Phys. Rev. B **45**, 13331 (1992).
[41] H. Ashraf, M. I. Arshad, S. M. Faraz, Q. Wahab, P. R. Hageman, and M. Asghar, J. Appl. Phys. **108**, 103708 (2010).
[42] P. A. Martin, B. G. Streetman, and K. Hess, J. Appl. Phys. **52**, 7409 (1981).
[43] G. Vincent, A. Chantre, and D. Bois, J. Appl. Phys. **50**, 5484 (1979).
[44] V. Karpus and V. Perel, Zh. Eksp. Teor. Fiz. **91**, 2319 (1986) [Sov. Phys. - JETP **64**, 1376 (1986)].
[45] S. D. Ganichev, I. N. Yassievich, W. Prettl, J. Diener, B. K. Meyer, and K. W. Benz, Phys. Rev. Lett. **75**, 1590 (1995).
[46] S. D. Ganichev, W. Prettl, and I. N. Yassievich, Phys. Solid State **39**, 1703 (1997).
[47] S. D. Ganichev, E. Ziemann, I. N. Yassievich, W. Prettl, A. A. Istratov, and E. R. Weber, Phys. Rev. B **61**, 10361 (2000).
[48] Q.-S. Zhu, H. Nagai, Y. Kawaguchi, K. Hiramatsu, and N. Sawaki, J. Vac. Sci. Technol. A **18**, 261 (2000).
[49] N. M. Johnson, W. Gotz, J. Neugebauer, and C. G. Van de Walle, Mater. Res. Soc. Symp. Proc. **395**, 723 (1996).
[50] W. Gotz, N. M. Johnson, D. P. Bour, M. D. McCluskey, and E. E. Haller, Appl. Phys. Lett. **69**, 3725 (1996).